Remote Sensing of Environment xxx (2014) xxx–xxx

Contents lists available at ScienceDirect

Remote Sensing of Environment

journal homepage: www.elsevier.com/locate/rse

Linking imaging spectroscopy and LiDAR with floristic composition and forest structure in Panama

Mark A. Higgins [a,*], Gregory P. Asner [a], Roberta E. Martin [a], David E. Knapp [a], Christopher Anderson [a], Ty Kennedy-Bowdoin [a], Roni Saenz [b], Antonio Aguilar [b], S. Joseph Wright [b]

[a] Department of Global Ecology, Carnegie Institution for Science, Stanford, CA 94305, USA
[b] Smithsonian Tropical Research Institute, Apartado 0843-0392, Balboa, Panama

ARTICLE INFO

Article history:
Received 11 June 2013
Received in revised form 23 September 2013
Accepted 30 September 2013
Available online xxxx

Keywords:
Imaging spectroscopy
LiDAR
Plant species composition
Forest structure
Panama
Tropical forest
Geology

ABSTRACT

Landsat and Shuttle Radar Topography Mission (SRTM) imagery have recently been used to identify broad-scale floristic units in Neotropical rain forests, corresponding to geological formations and their edaphic properties. Little is known about the structural and functional variation between these floristic units, however, and Landsat and SRTM data lack the spectral and spatial resolution needed to provide this information. Imaging spectroscopy and LiDAR (Light Detection and Ranging) have been used to measure canopy structure and function in a variety of ecosystems, but the ability of these technologies to measure differences between compositionally-distinct but otherwise uniform tropical forest types remains unknown. We combined 16 tree inventories from central Panama with imaging spectroscopy and LiDAR elevation data from the Carnegie Airborne Observatory to test our ability to identify patterns in plant species composition, and to measure the spectral and structural differences between adjacent closed-canopy tropical forest types. We found that variations in spectroscopic imagery and LiDAR data were strong predictors of spatial turnover in plant species composition. We also found that these compositional, chemical, and structural patterns corresponded to underlying geological formations and their geomorphological properties. We conclude that imaging spectroscopy and LiDAR data can be used to interpret patterns identified in lower resolution sensors, to provide new information on forest function and structure, and to identify underlying determinants of these patterns.

1. Introduction

Imaging spectroscopy and LiDAR (Light Detection and Ranging) have become powerful tools in the study of ecosystems. Unlike multispectral sensors such as Landsat or the Moderate Resolution Imaging Spectroradiometer (MODIS), which integrate reflectance in visible to shortwave wavelengths over a relatively small number of broad-bandwidth spectral channels, imaging spectroscopy measures reflected electromagnetic radiation on a continuous narrow-band (e.g. 10 nm) basis. This provides spectra for detailed analysis of remotely-sensed features and hence diagnosis of their chemical properties (Kokaly, Asner, Ollinger, Martin, & Wessman, 2009; Ustin et al., 2009). From airborne data, these features may resolve forest plots or individual tree crowns. LiDAR data are equally useful for studying ecosystems. LiDAR is an active sensing system in which return times for laser emissions are used to calculate the elevation of both terrain and aboveground features. In forested ecosystems, LiDAR returns can penetrate the canopy and provide information from both the ground and multiple points within the forest canopy (Dubayah et al., 2010). These data can then be used to generate high-resolution images of forest structure, allowing estimates of forest properties such as canopy height and biomass (Drake, Dubayah, Knox, Clark, & Blair, 2002; Lefsky, Cohen, Parker, & Harding, 2002).

Imaging spectroscopy and LiDAR data have been used in a variety of ecosystems to study vegetation composition, structure, and dynamics. Both spectroscopy and LiDAR data have individually been used to predict species richness in temperate forests (Leutner et al., 2012), tropical forests (Carlson, Asner, Hughes, Ostertag, & Martin, 2007; Kalacska et al., 2007; Wolf et al., 2012), savannas (Cho et al., 2012), and tropical mangrove ecosystems (Held, Ticehurst, Lymburner, & Williams, 2003). In addition, imaging spectroscopy has been used to identify changes in species composition in savanna (Baldeck & Asner, 2013), temperate grassland (Schmidtlein & Sassin, 2004; Schmidtlein, Zimmermann, Schupferling, & Weiss, 2007), and mixed forest/non-forest ecosystems (Leutner et al., 2012); and imaging spectroscopy has been used to map the distributions of individual species in tropical forests and savannas (Asner & Vitousek, 2005; Clark, Roberts, & Clark, 2005; Feret

* Corresponding author at: Department of Global Ecology, Carnegie Institution for Science, 260 Panama Street, Stanford, CA 94305, USA. Tel.: +1 805 350 1141.
E-mail address: higginsm@stanford.edu (M.A. Higgins).

http://dx.doi.org/10.1016/j.rse.2013.09.032
0034-4257/

& Asner, 2012). LiDAR data are particularly suited to studying forest structure and dynamics, and has been used to identify patterns in biomass (Asner, Hughes, Varga, Knapp, & Kennedy-Bowdoin, 2009; Clark, Roberts, Ewel, & Clark, 2011; Drake et al., 2002), ecosystem development (Kellner et al., 2011), and successional dynamics (Castillo, Rivard, Sanchez-Azofeifa, Calvo-Alvarado, & Dubayah, 2012; Dubayah et al., 2010) in tropical forests. Most promisingly, LiDAR and imaging spectroscopy data have been fused to yield improved estimates of species richness, species distributions, and forest biomass in savanna and forest ecosystems (Asner et al., 2008; Cho et al., 2012; Colgan, Baldeck, Feret, & Asner, 2012; Lucas, Lee, & Bunting, 2008).

We have recently shown that medium-resolution data from Landsat and the Shuttle Radar Topography Mission (SRTM) can be used to infer floristic discontinuities in northwestern Amazonia, corresponding to geological formations and their edaphic properties (Higgins et al., 2011, 2012). Similar relationships between soils and forest composition in Central America and Asia also suggest that these patterns might be widespread (Jones et al., 2013; Palmiotto et al., 2004). Due to the limited spatial and spectral resolution of Landsat and SRTM data, however, we have been unable to determine whether these compositional discontinuities are translated into patterns in forest structure and functional properties.

Here we propose that imaging spectroscopy and LiDAR may be used both to identify changes in plant species composition, and to provide detailed information about the functional and structural differences between compositionally-defined forest types. To evaluate this possibility, we combined field inventories of plant species composition from a tropical forest in central Panama with spectral and LiDAR data from the Carnegie Airborne Observatory Airborne Taxonomic Mapping System (CAO-AToMS) (Asner, Knapp, et al., 2012). CAO-AToMS incorporates a dual-channel waveform LiDAR with a 428-channel Visible to Shortwave Infrared (VSWIR) imaging spectrometer, providing orthorectified 1 m and 2 m resolution data, respectively, when flown at 2000 m above ground level (a.g.l.).

We concentrated our study on a boundary between two geological formations. Our objectives were (1) to test the ability of imaging spectroscopy and LiDAR to detect changes in plant species composition between these formations; (2) to compare these formations on the basis of forest canopy structure and spectra as identified from LiDAR and VSWIR data; and (3) to examine the relationship between geology or geomorphology and patterns in canopy reflectance and structure. To our knowledge, this is the first time that imaging spectroscopy or LiDAR data have been tested for its ability to detect and study compositionally-defined types in tropical forests.

2. Materials and methods

2.1. Study area

We focused our data collection on a boundary between the Ocú and Gatuncillo geological formations in central Panama (Fig. 1), at a site characterized by unbroken, tropical broadleaf rainforest. The Ocú Formation dates approximately to the Paleocene and consists of uplifted limestone and volcanic tuff extending north and east into the Panamanian cordillera (MICI, 1990). The younger Gatuncillo Formation dates to the middle to late Eocene, and consists of younger sedimentary material deposited at the base of the Ocú Formation, including mudstone, shale, quartz sandstone, and algal and foraminiferal limestone (MICI, 1990). We did not collect soil data for our study sites, but previous soil sampling suggests that cation exchange capacity and base cation concentrations are higher on the Alfisols of the Gatuncillo Formation than the Oxisols of the Ocú Formation (Ben Turner, personal communication). Elevation in our study area ranges from 45 m to 261 m, and is not considered sufficient to create biologically-significant variations in climate over the area studied here. We collected airborne imaging spectroscopy and LiDAR data for the study area, and sampled it in the field for plant species composition.

2.2. CAO-AToMS data

We used CAO-AToMS to acquire co-aligned VSWIR and LiDAR data for the study area in February 2012. The landscape was imaged by 20 parallel and overlapping flight lines, approximately 1 km wide and 22 km long, running from the northwest to the southeast, and overlapping

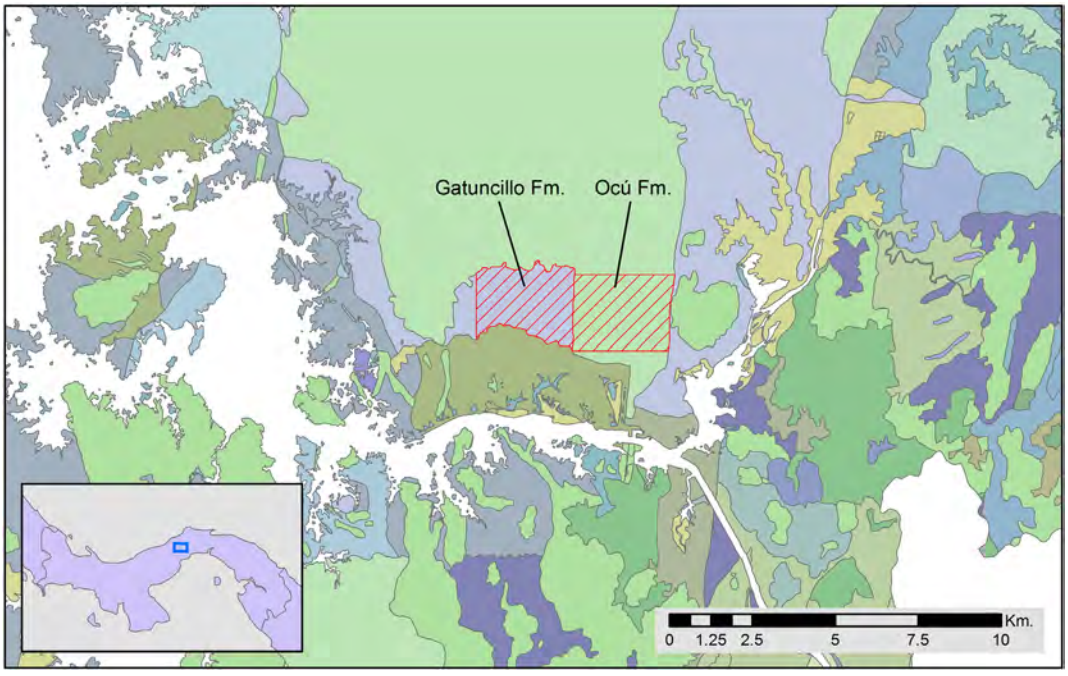

Fig. 1. Location of study area relative to geological map of Panama. Red cross-hatching indicates extent of study area, divided into two halves corresponding to the Gatuncillo and Ocú Formations. Study area is superimposed on the national geological map of Panama (MICI, 1990); inset indicates location of map relative to Panama country boundaries. (For interpretation of the references to color in this figure legend, the reader is referred to the web version of this article.)

Please cite this article as: Higgins, M.A., et al., Linking imaging spectroscopy and LiDAR with floristic composition and forest structure in Panama, *Remote Sensing of Environment* (2014), http://dx.doi.org/10.1016/j.rse.2013.09.032

by 50%. LiDAR data were available for all flight lines, but cloud-free VSWIR data were available only for six flight lines in the center and the east of our study area. As such, cloud-free VSWIR data were not available for the southwestern corner of our study area. Prior to analysis, we subset both the LiDAR and VSWIR datasets to the extent of the study area (Figs. 2, 3).

The VSWIR data consisted of 2 m resolution canopy reflectance measurements covering the 380 nm to 2512 nm wavelength range in 428 channels of 5 nm sampling (full-width, half-maximum). These data were then resampled to 214 bands of 10 nm bandwidth to reduce data volume and facilitate spectroscopic analysis. Prior to analysis, the VSWIR data were corrected for atmospheric distortions and bidirectional reflectance distribution function (BRDF) effects (Colgan et al., 2012). For visualization and analysis of the VSWIR data, we omitted bands coinciding to regions of high absorption by water vapor (1320 to 1500 nm, and 1770 to 2010 nm), and removed pixels corresponding to clouds and shaded canopy. Clouds were masked manually and shaded pixels were identified by an algorithm that considered both sun location and height of neighboring pixels derived from the LiDAR data, resulting in the removal of about 50% of pixels for the study area (Asner et al., 2007).

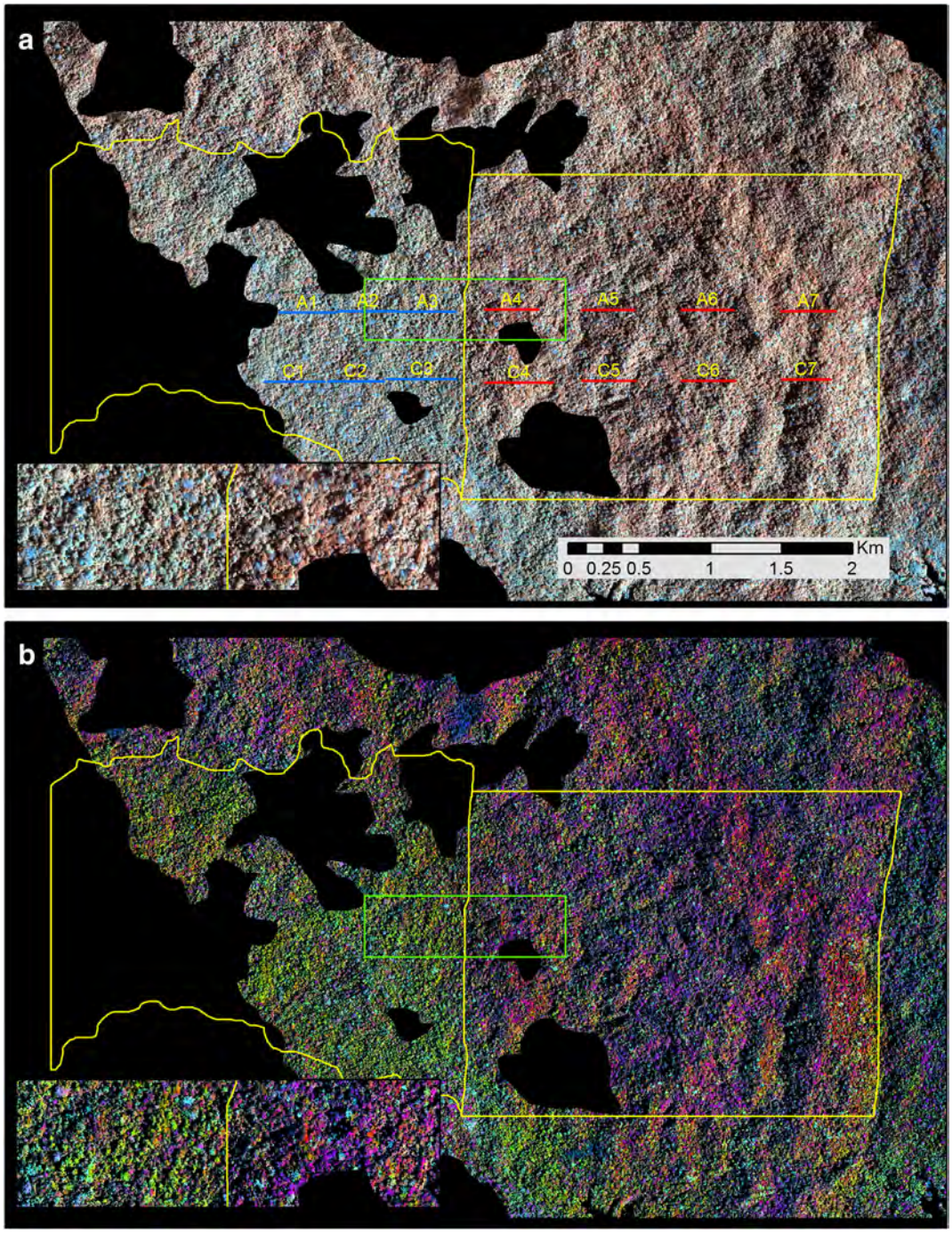

Fig. 2. VSWIR imagery for study area, superimposed with results of clustering analysis. (a) Original VSWIR imagery, with 830, 1650, and 2220 nm set to red, green, and blue, respectively. (b) Principal component transformation of VSWIR data, with PCs 1, 2, and 3 set to red, green, and blue, respectively. Superimposed on (a) are the locations of the 16 tree inventories and their classification into two groups by clustering analysis (red and blue). Insets in the lower left of both panels are magnifications of the areas in the green boxes, and the yellow lines indicate the extent of the study area shown in Fig. 1. Dark patches within images are areas where clouds have been removed. (For interpretation of the references to color in this figure legend, the reader is referred to the web version of this article.)

Please cite this article as: Higgins, M.A., et al., Linking imaging spectroscopy and LiDAR with floristic composition and forest structure in Panama, *Remote Sensing of Environment* (2014), http://dx.doi.org/10.1016/j.rse.2013.09.032

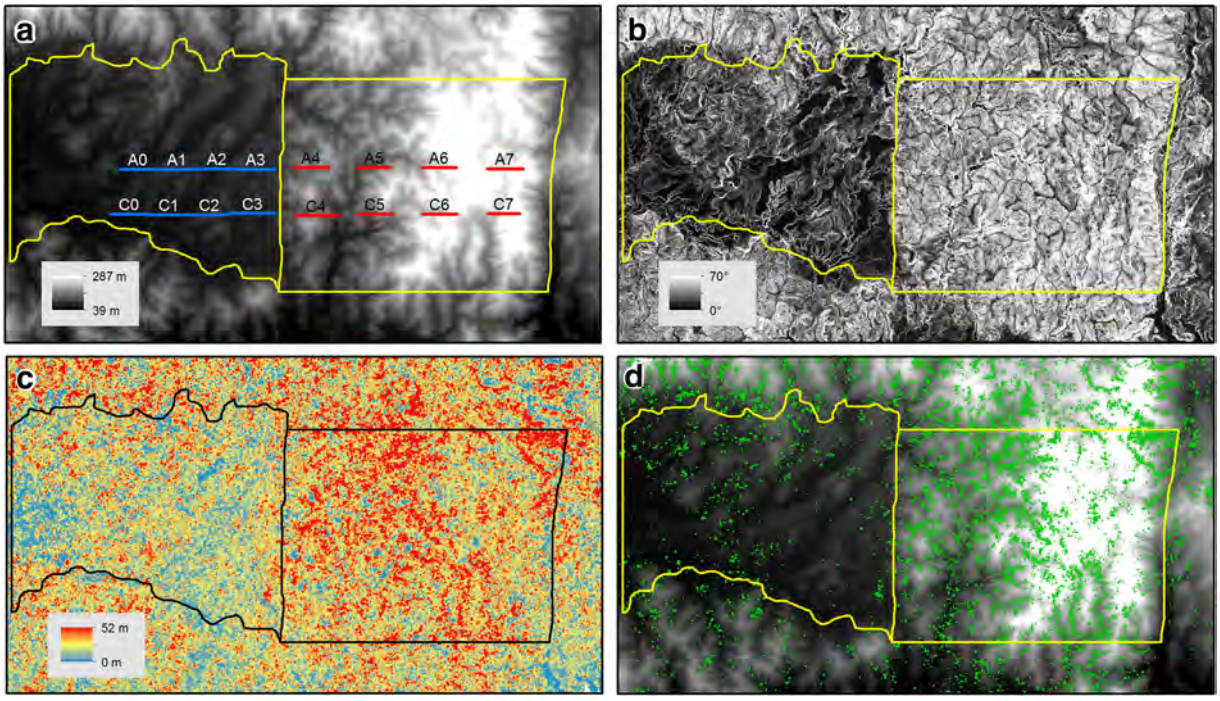

Fig. 3. LiDAR data for study area, superimposed with results of clustering analysis. (a) Terrain elevation data for study area, where lighter tones indicate higher elevations. (b) Slope for study area, where lighter tones indicate steeper slopes. (c) Mean canopy height for study area, where warmer tones indicate higher canopy. (d) LiDAR returns in the 37–38 m height class, where green indicates the presence of vegetation of any density in this class. Superimposed on (a) are the locations of the 16 tree inventories and their classification into two groups by clustering analysis (red and blue). Yellow or black lines indicate the extent of the study area shown in Fig. 1. (For interpretation of the references to color in this figure legend, the reader is referred to the web version of this article.)

For this study, we used the discrete-return portion of the LiDAR data, providing a maximum of four returns per laser shot, to calculate both ground elevation at 1 m resolution, and mean canopy height (MCH) at 5 m resolution. Because the data were collected by flying adjacent flightlines with 50% overlap, the LiDAR data density was two laser shots per square meter on the ground. To calculate ground elevation, the flight area was divided into 100 m kernels and within each kernel the lowest elevation return was classified as ground. Neighboring returns were classified iteratively, such that if the nearest unclassified return was <5.5° and 1.5 m higher in elevation, it was classified as ground (Asner et al., 2013). This process was repeated until all points within the kernel were classified, after which all ground returns were used to generate a triangulated irregular network (TIN) which was converted to a raster surface at 1 m resolution, with a height accuracy of 10 cm. To calculate mean canopy height, the flight area was divided into 5 m by 5 m pixels, and all returns greater than 50 cm above ground within each pixel were averaged, so as to eliminate possible ground returns. Last, we used ground elevation data to calculate degrees slope at 1 m resolution (calculated in ArcGIS v10; ESRI, Redlands, California, USA).

2.3. Tree inventory data

We collected data on tree species composition along 16 linear transects, organized along two east–west lines that crossed the boundary between the Ocú and Gatuncillo Formations. These lines were labeled "A" and "C" and transects were numbered from 0 to 7, west to east along these lines (Figs. 2, 3). These transects were divided equally between the geological formations, such that eight transects were sampled in each formation (Figs. 2, 3). Along each transect we identified all trees ≥10 cm diameter at breast height (dbh) to species and produced species lists for each site. The transects were either 6 m × 400 m (14 transects) or 5 m × 500 m (2 transects, "C3" and "C4"), with an average area of 0.24 ha. This area was selected to sample approximately 100 stems per transect, the minimum number identified by Higgins and Ruokolainen, (2004) for identifying compositional patterns in Neotropical forests. We collected a minimum of five GPS points per transect and used these to geolocate the transects for comparison to the VSWIR and LiDAR imagery.

2.4. CAO data analysis

Principal component analysis (PCA) was used to reduce the 214 bands of VSWIR data to three synthetic axes for comparison to the compositional and LiDAR data (analysis performed with ENVI Version 4.8, Excelis Visual Information Solutions, Virginia, USA). We also selected three VSWIR channels—830 nm, 1650 nm, and 2220 nm—for comparison to the compositional and LiDAR data. These channels were chosen because they are at the center of the near infrared (NIR), shortwave infrared 1 (SWIR 1), and shortwave infrared 2 (SWIR 2) bands of the Landsat sensor (bands 4, 5, and 7, respectively). These bands are interesting because they have previously been used in Landsat data to identify patterns in plant species composition (Higgins et al., 2011, 2012; Tuomisto, Poulsen, et al., 2003; Tuomisto, Ruokolainen, Aguilar, & Sarmiento, 2003). In addition, to compare the full reflectance spectra of the transects, we calculated the mean spectrum for each transect for each of the 214 channels using the transect outlines described below (Section 2.6).

2.5. Tree inventory data analysis

We used clustering analysis to visualize patterns in plant species composition relative to the geological formations and CAO AToMS imagery. For this purpose we calculated floristic dissimilarities between sites using the Jaccard index (Jones et al., 2013), and then divided the tree transects into two groups using the unweighted pair-group method (UPGMA; Legendre & Legendre, 1998; Tuomisto, Ruokolainen, et al., 2003). We additionally used nonmetric multidimensional scaling (NMDS) to reduce

Please cite this article as: Higgins, M.A., et al., Linking imaging spectroscopy and LiDAR with floristic composition and forest structure in Panama, *Remote Sensing of Environment* (2014), http://dx.doi.org/10.1016/j.rse.2013.09.032

the pattern of compositional similarities and differences between sites, as measure by the Jaccard index, to a single ordination axis for comparison to individual VSWIR bands; individual VSWIR PCA axes; or terrain variables generated from the LiDAR data. Clustering and NMDS analyses were performed with PC-ORD v. 4.41 (MjM Software, Gleneden Beach, OR, USA).

2.6. Relationships between tree species composition, VSWIR variables, and LiDAR variables

First, to test the ability of VSWIR and LiDAR data to predict variations in tree species composition, we calculated the correlation between NMDS values, as the dependent variable; and mean values of either elevation, MCH, the three individual VSWIR bands noted above, or the three VSWIR PCA axes (Section 2.4), as independent variables. To calculate mean values for each transect for LiDAR and VSWIR variables, we delineated outlines for the transects and then calculated the mean value for all pixels within this area, excluding shaded and clouded pixels for the VSWIR data. In addition, VSWIR data were not available for two transects, A0 and C0, and these transects were omitted from analyses that included VSWIR data.

Second, to verify the ability of VSWIR and LiDAR data to measure differences in forest chemistry and structure between compositionally-defined forest types, we compared spectra for the two groups defined by our clustering analysis for all 16 transects. We additionally calculated the mean MCH for each clustering group, based on the data for the 16 transects, and tested the difference between the mean values for the two groups.

Third, to identify possible determinants of canopy composition, structure, and chemistry, we calculated the correlations between NMDS values, VSWIR values (bands and PCA axes), and MCH, as dependent variables; and elevation and slope, as measured by the LiDAR data, as independent variables. We conducted these analyses both using values for the tree transect areas; and for the full extents of the Ocú and Gatuncillo Formations in our study area, for LiDAR variables only. For analyses including the full study area, we resampled elevation, slope, and MCH data to 100 m resolution, and computed the relationships amongst these variables for all 100 m pixels across the full study area.

As a result of these analyses we effectively calculated all possible correlations between three sets of variables: tree species composition, represented by a single NMDS axis; VSWIR variables, consisting of three bands and three principal components; and LiDAR variables, consisting of elevation, slope, and mean canopy height. All correlations were reported as the coefficient of determination (r^2).

3. Results

3.1. Patterns in CAO-AToMS data

We observed clear discontinuities in the VSWIR and LiDAR data, corresponding to the boundary between the Ocú and Gatuncillo Formations (Figs. 2–4). Using VSWIR bands 830 nm, 1650 nm, and 2220 nm set to red, green, and blue, the Gatuncillo Formation was characterized by blue tones and the Ocú Formation by red tones (Fig. 2a). These differences were pronounced after a principal component transformation of the VSWIR data (Fig. 2b). Setting PCA axes one, two, and three to red, green, and blue, the Gatuncillo Formation was characterized by neon green and yellow tones, and the Ocú Formation was characterized by bright magenta tones. In both untransformed and transformed images, these changes in tone aligned precisely with the north–south boundary between the two geological formations.

We also observed abrupt differences between the two formations in the LiDAR elevation data. Using the areas delineated in Fig. 1, and resampling the LiDAR data to 100 m, we found that the mean elevation of the Ocú Formation was 143 m, an average of 80 m greater than the Gatuncillo Formation (mean elevation 63 m; Fig. 3a). In addition, slopes at the Ocú Formation were twice as steep as that in the Gatuncillo Formation, averaging 25.5 and 11.4° respectively (Fig. 3b). These differences in landscape position and slope corresponded to a 20% (3.75 m) difference in mean canopy height between the taller Ocú Formation

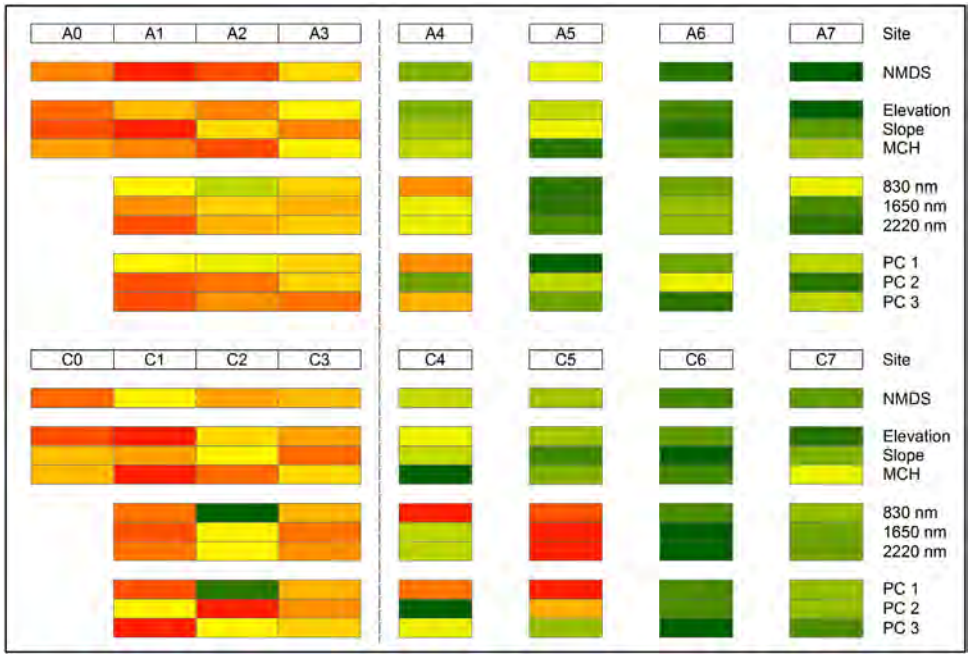

Fig. 4. Summary of floristic, LiDAR, and VSWIR data for tree inventories. Color of boxes indicates values of floristic (NMDS), LiDAR (elevation, slope, and MCH), and VSWIR (830, 1650, and 2220 nm; and PC 1, 2, and 3) variables for inventory areas along line "A" or "C". Green tones indicate lower values, with the exception of the LiDAR variables and VSWIR PC 3 for which green tones indicate higher values. Broken gray line indicates boundary between Ocú and Gatuncillo Formations. (For interpretation of the references to color in this figure legend, the reader is referred to the web version of this article.)

Please cite this article as: Higgins, M.A., et al., Linking imaging spectroscopy and LiDAR with floristic composition and forest structure in Panama, *Remote Sensing of Environment* (2014), http://dx.doi.org/10.1016/j.rse.2013.09.032

(22.12 m) and the Gatuncillo Formation (18.37 m; Fig. 3c). On average the Ocú Formation was higher, steeper, and supported taller forests than the Gatuncillo Formation.

3.2. Patterns in tree inventory data

We inventoried tree species at 16 sites, for a total of 1860 individuals and 147 species. On average we encountered 116 individuals and 37 species per site, with a range of 96 to 176 individuals per transect and 31 to 44 species. Three transects had less than 100 individuals: A1, C0, and C6; with 96, 96, and 97 species, respectively.

Clustering analysis of our tree inventory data divided the tree transects into two groups corresponding exactly to the geological formations (Figs. 2, 3). The average difference in species between transects from different groups was 79% (Jaccard index), but the species turnover between transects within the same geological formation was also high (66% for the Ocú Formation and 72% for the Gatuncillo Formation). NMDS ordination of our tree inventories yielded a single axis that explained 68% of the variation in the original dataset (Fig. 4). We considered this axis representative of the dominant compositional pattern in the data, and used it for comparison to the VSWIR and LiDAR data.

3.3. Relationships between tree species composition, VSWIR variables, and LiDAR variables

Individual VSWIR bands or principal components, respectively, predicted up to 47% and 67% of the floristic variation in the study area (1650 nm and PC2, respectively; Table 1), as measured by the NMDS axis. These bands and components varied substantially in their ability to predict compositional patterns, however, such that variations in the 830 nm band and PC1 were not correlated with variations in composition, while the remaining bands and components were strongly correlated with composition (Table 1; Fig. 4). LiDAR terrain and structural variables also predicted variations in plant species composition (Table 2), such that slope and elevation explained 80% and 75% of NMDS scores in the study area, respectively, indicating strong environmental control of species composition as discussed below.

Furthermore, though transect C5 was similar in species composition to other transects in the Ocú Formation, it differed substantially in reflectance (Figs. 4, 5). Reflectance values for C5 at 1650 nm, 2220 nm, and PC1 were greater than all other transects, including transects in the Gatuncillo Formation. This difference was clear when comparing spectra for all 16 transects, such that C5 demonstrated anomalously high reflectance in visible wavelengths, SWIR1, and SWIR 2 (Fig. 5, dashed lines). The range of values for C5 for 1650 nm, 2220 nm, and PC1, furthermore, was substantially greater than for any other transect. These results suggested that C5 was an outlier due to mixed or unusual conditions, and we thus additionally calculated all correlations between the VSWIR data and other variables in the absence of C5. After excluding C5, individual bands and principal components were able to predict up to 76% of the variation in plant species composition (2220 nm and PC2) as measured by NMDS values.

The VSWIR and LiDAR sensors also detected clear differences in canopy spectral and structural characteristics between the two floristic groups identified in the clustering analysis. With the exception of transect C5, spectra for the two forest types were completely separated in SWIR1 and SWIR 2 spectral regions, and strongly separated in the visible wavelengths, consistent with the correlations observed above between the compositional and spectral data (Table 1). We also observed clear differences between the two forest types in canopy structure, such that forests growing on the Ocú Formation were 22% taller on average than forests on the Gatuncillo Formation (MCH of 22.6 and 18.6 m, respectively; $P < 0.01$). These findings were consistent with the differences observed above using 100 m data for the full study area (Section 3.1).

These compositional and chemical patterns correlated with underlying variations in geomorphology. Elevation and slope explained 75% and 80%, respectively, of the variation in NMDS values amongst the 16 transects. Elevation also explained up to 59% and 63% of the variation in individual VSWIR bands or principal components, respectively, and slope explained up to 46% and 75% (1650 nm and PC 3 in both cases; Table 1). Individual bands and PCs varied in their correlations with terrain, however, such that reflectance at 830 nm and PC 1 were poorly correlated with elevation and slope, while reflectance in other bands or PCs was strongly correlated.

Elevation and slope also explained variations in canopy structure. Using 100 m data for the area delineated in Fig. 1, elevation explained 40% of the variation in MCH, but this relationship was nonlinear, such that the tallest trees were found at intermediate elevations in the Ocú Formation (second-order polynomial; Fig. 6a). These positions in the Ocú Formation corresponded to the areas of highest slope, such that we observed a strong linear relationship between slope and mean canopy height, and a non-linear relationship between elevation and slope (Fig. 6b, c). Generally, the tallest trees in our study area were found neither on flat lowlands or high ridgetops, but rather on the steep slopes of the Ocú Formation (Fig. 3d). These findings indicate both differences in canopy height between the two formations, and variations within the Ocú Formation due to topographic position.

Stronger relationships were observed when considering only the 16 transects, using the original 1 and 5 m resolution LiDAR data. Based on the transect areas, elevation and slope explained 75% and 59% of the variation in MCH, and elevation and slope were strongly correlated ($r^2 = 0.88$, second-order polynomial). To complete our analyses, we calculated the relationship between MCH and individual VSWIR bands or principal components, and found that forest structure and reflectance were strongly correlated, with the exception of 830 nm and PC 1 (Table 2).

Table 2
Correlations (r^2) amongst LiDAR variables and NMDS scores. All correlations significant at $P < 0.05$.

	NMDS	MCH	Slope
Elevation	0.75	0.75 [a]	0.88 [a]
Slope	0.80	0.59	
MCH	0.40		

[a] Indicates that correlation was calculated using a second-order polynomial, where elevation was the independent variable.

4. Discussion

Using 16 sites in central Panama, we found that imaging spectroscopy and LiDAR data from the CAO-AToMS system were able to detect

Table 1
Correlations (r^2) between VSWIR variables and NMDS scores or LiDAR variables. All correlations significant at $P < 0.05$ unless indicated with italics. Value in parentheses indicates correlation in absence of transect C5.

	830 nm	1650 nm	2220 nm	PC1	PC2	PC3
NMDS	*0.00 (0.00)*	0.47 (0.65)	0.46 (0.76)	*0.07 (0.11)*	0.67 (0.76)	0.55 (0.55)
Elevation	*0.06 (0.07)*	0.59 (0.74)	0.54 (0.77)	*0.22 (0.26)*	0.54 (0.57)	0.63 (0.63)
Slope	*0.02 (0.07)*	0.46 (0.87)	0.37 (0.88)	*0.14 (0.31)*	0.50 (0.70)	0.75 (0.77)
MCH	*0.01 (0.02)*	0.41 (0.59)	0.38 (0.66)	*0.1 (0.16)*	0.47 (0.55)	0.54 (0.54)

Please cite this article as: Higgins, M.A., et al., Linking imaging spectroscopy and LiDAR with floristic composition and forest structure in Panama, *Remote Sensing of Environment* (2014), http://dx.doi.org/10.1016/j.rse.2013.09.032

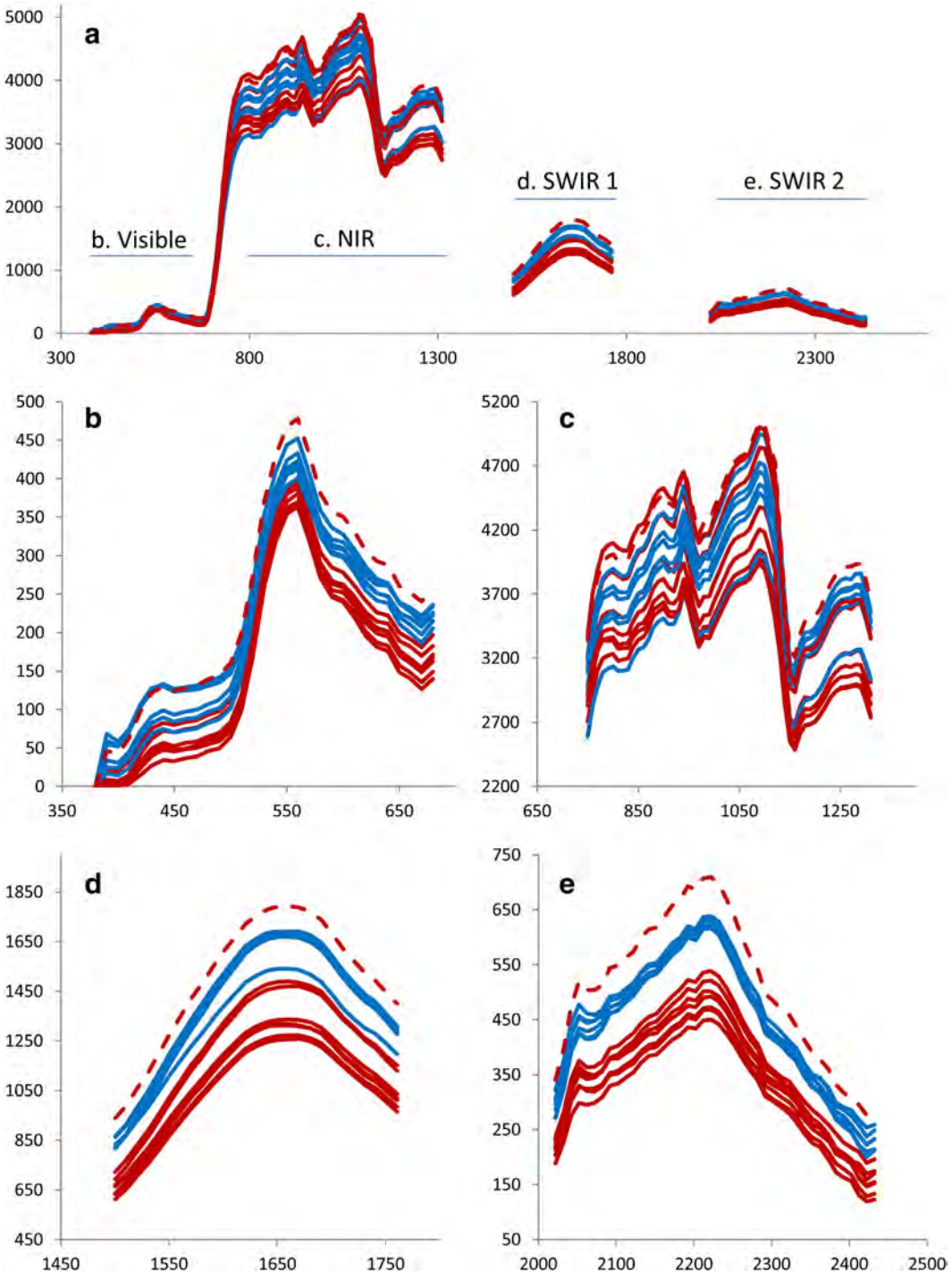

Fig. 5. Mean spectra for 16 tree inventories, colored by clustering group. (a) Full spectra for the 16 plant transects. (b) to (e) Magnifications of visible, near infrared (NIR) and shortwave infrared (SWIR 1 and 2) portions of the full spectra, as indicated in (a). Spectra are colored according to the two clustering groups (red and blue), consistent with Figs. 2 and 3. Broken line indicates the outlying transect C5. (For interpretation of the references to color in this figure legend, the reader is referred to the web version of this article.)

turnover in plant species composition in otherwise uniform closed-canopy and tall tropical forest. Variations in VSWIR imagery predicted up to 67% of the variation in tree species composition in the study area, as measured by a single NMDS axis, and this rose to 76% after the removal of an outlying site. Variations in LiDAR data, furthermore, predicted up to 80% of this variation in composition. In addition, we found that imaging spectroscopy and LiDAR could be used to measure differences in canopy spectral properties and structure between compositionally distinct forest types. Based on VSWIR data we found nearly complete spectral separation between two geologically-defined forest types in the shortwave infrared, strongly suggestive of differences in canopy chemical properties (Asner et al., 2011). We also observed a 22% change in mean canopy height, indicating differences in both forest structure and likely biomass (Asner, Mascaro, et al., 2012; Clark et al., 2011; Drake et al., 2002). These findings demonstrate the ability of imaging spectroscopy and LiDAR data both to map variations in plant species composition, and to measure chemical and structural differences between forest types.

Our findings also illustrate the ability of LiDAR and imaging spectroscopy to identify possible determinants of these compositional, spectral,

Please cite this article as: Higgins, M.A., et al., Linking imaging spectroscopy and LiDAR with floristic composition and forest structure in Panama, *Remote Sensing of Environment* (2014), http://dx.doi.org/10.1016/j.rse.2013.09.032

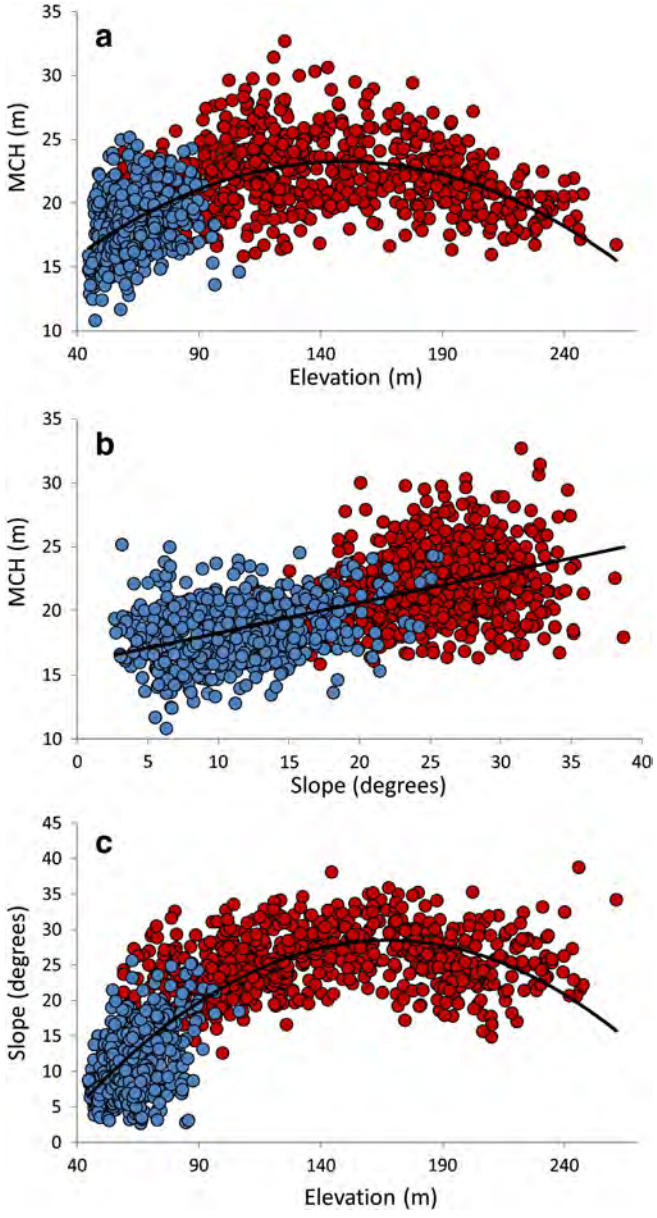

Fig. 6. Relationships between elevation, slope, and mean canopy height (MCH) for study area. Points represent values for individual 100 m pixels for full study area and colors indicate the geological formation in which the pixel is located (blue corresponds to Gatuncillo Formation, and red corresponds to Ocú Formation), consistent with Figs. 2 and 3. Black lines indicate linear (a, b) or second-order polynomial (c) regressions. Coefficients of determination (r^2) for regressions are (a) 0.40, (b) 0.36, and (c) 0.69. (For interpretation of the references to color in this figure legend, the reader is referred to the web version of this article.)

and structural patterns. Elevation predicted 75% of the variation in plant species composition as represented by NMDS scores, consistent with the 73% reported by Higgins et al. (2012) for SRTM data in northwestern Amazonia. In addition, elevation also explained 75% of the variation in mean canopy height, consistent with earlier findings in Colombia (Asner, Clark, et al., 2012), and up to two-thirds of variation in canopy reflectance. As in Amazonia, we do not believe that elevation is directly responsible for these patterns, through for example changes in air temperature or climate. Instead, elevation is a strong predictor of underlying geology ($r2 = 0.71$, $p < 0.001$), and these patterns may be due to a change in soil properties between vertically stratified geological formations, consistent with recent findings for both Panama and Peru (Asner et al., 2010; Higgins et al., 2011; Jones et al., 2013).

In addition, our data suggest that geomorphological variation within geological formations may also be important to regulating forest properties. Slope explained 80% of the change in plant species composition (i.e. NMDS scores) and 59% of the variation in mean canopy height in our study area, and up to three-quarters of the variation in canopy reflectance. Both mean canopy height and slope peaked at intermediate elevations, corresponding to the steep slopes of drainages in the Ocú Formation. This relationship between slope and forest structure is consistent with previous studies in Panama, and suggests that factors influenced by slope—including soil texture, regions of nutrient accumulation, or soil drainage—may also be important in controlling forest properties (Condit, Engelbrecht, Pino, Perez, & Turner, 2013; John et al., 2007; Mascaro et al., 2011). It should be noted, however, that at greater slopes than observed in our study area, we might expect reduced canopy heights due to increased mortality from mudslides and treefall (Ren, Leslie, & Duan, 2012).

Based on the data reported here, however, we are not able to conclude whether geology or slope plays a larger role in regulating forest properties in the study area, or whether these properties are instead due to unmeasured variables such as land-use history. Elevation and geology are both strongly correlated with slope ($r^2 = 0.88$ for both, $p < 0.001$), making it impossible to separate the relative importance of these variables to regulating canopy composition, structure, or reflectance. In practical terms, this means that we have few examples of low slope in the Ocú Formation or high slope in the Gatuncillo Formation. To disentangle the relative importance of geology and slope to forest properties, we recommend a larger study area incorporating more variation in slope within these two formations.

In addition, it is possible that the patterns observed here reflect differences in land-use history rather than geology or slope. The Panama Canal area has a long history of human use, and old growth forest is scarce in the region (Ibanez et al., 2002). Though no reliable land-use records are available for our study area, human habitation or clearing for agriculture may have been concentrated on the lower-elevation and lower-slope areas in the west of our study area. It is thus possible that the patterns in forest structure and composition reflect recovery from past disturbance rather than direct control by geology and geomorphology. This would explain elevated abundances of young-forest species in the Gatuncillo Formation, such as *Gustavia superba* (64% more abundant than expected), *Attalea butyracea* (81%), and *Terminalia amazonia* (73%); and old-forest species in the Ocú Formation, such as *Heisteria concinna* (86%), *Socratea exorrhiza* (100%), and *Trichilia tuberculata* (25%).

This said, the close association of patterns in species composition, canopy reflectance, and forest structure to geology and geomorphology suggests that these are important underlying drivers of these patterns. Deep within the Ocú Formation we consistently see variation in these variables along slope gradients that are unlikely due to human intervention. In addition, we observe clear changes in plant species composition and VSWIR imagery across the Ocu–Gatuncillo border, both in the east and north, which are difficult to explain strictly on the basis of human disturbance. Whatever the case, sensor systems such as CAO-AToMS can be used to identify these patterns, guide sampling in the field, and provide data to test the importance of possible determinants.

The findings from the VSWIR sensor come with one important caveat. Due to the number of species sampled, and the time and expense of collecting and processing leaf samples for chemistry, we could not calibrate the spectral signatures for our plant inventories to chemical properties. In light of the consistent differences between the two geological formations, however, and previous studies in tropical forests, we are confident that these spectral differences reflect changes in canopy chemistry (Asner & Martin, 2011; Asner et al., 2011; Sanchez-Azofeifa et al., 2009). Transects from the two geological formations were indistinguishable in the near-infrared, suggesting that forests on these formations do not differ substantially in total leaf area volume or LAI (Myneni, Nemani, & Running, 1997). However,

Please cite this article as: Higgins, M.A., et al., Linking imaging spectroscopy and LiDAR with floristic composition and forest structure in Panama, *Remote Sensing of Environment* (2014), http://dx.doi.org/10.1016/j.rse.2013.09.032

these formations did clearly differ in reflectance in the SWIR1 and SWIR2 regions, such that the Gatuncillo Formation exhibited consistently higher reflectance values than the Ocú Formation. This difference suggests lower leaf mass per area (LMA) and lower defense compound chemical investment on the Gatuncillo Formation (Asner et al., 2011). In addition, transects from the two formations were largely separable in the visible wavelengths, such that the Gatuncillo Formation again had higher reflectance, indicating greater investment in chlorophyll and nitrogen concentrations in foliage (Kokaly et al., 2009; Ustin et al., 2009). These differences are consistent with a growth-defense tradeoff scenario in which forests on the nutrient-poor Ocú Formation allocate to nutrient acquisition and leaf defenses, while forests on the more nutrient-rich Gatuncillo Formation are free to allocate to light acquisition and growth. This hypothesis can be tested by soil sampling across these two geological formations.

Last, a comparison of our findings with earlier studies of medium-resolution sensors such as Landsat and SRTM reveals the complementary nature of these high and medium-resolution systems, and suggests an efficient strategy for deploying airborne sensors. Variations in Landsat imagery and SRTM elevation data have previously been found to be correlated with variations in plant species composition at sites in northwestern Amazonia (Higgins et al., 2012; Salovaara, Thessler, Malik, & Tuomisto, 2005; Tuomisto, Poulsen, et al., 2003; Tuomisto, Ruokolainen, et al., 2003), consistent with our findings for VSWIR imagery and LiDAR elevation data. This indicates that both medium and high-resolution sensors can be used to identify patterns in plant species composition in tropical forests. The sensors described here, however, also allow the measurement of forest properties such as canopy structure and chemistry, but at the cost of higher expense and smaller footprints. This suggests that airborne sensors could be most efficiently used by first using lower-resolution sensors such as Landsat and SRTM to identify broad-scale patterns; and then targeting high-resolution sensors to areas of rapid turnover. This combination of sensing systems could provide the information on forest structure and chemistry needed to understand the dynamics, functioning, and resilience of tropical forests.

Acknowledgments

Data collection and analysis were supported by the Grantham Foundation for the Protection of the Environment and the endowment of the Carnegie Institution for Science. The Carnegie Airborne Observatory is made possible by the Gordon and Betty Moore Foundation; the Grantham Foundation for the Protection of the Environment; the John D. and Catherine T. MacArthur Foundation; the Avatar Alliance Foundation; the W. M. Keck Foundation; the Margaret A. Cargill Foundation; Mary Anne Nyburg Baker and G. Leonard Baker Jr.; and William R. Hearst III.

References

Asner, G. P., Clark, J. K., Mascaro, J., Garcia, G. A. G., Chadwick, K. D., Encinales, D. A. N., et al. (2012). High-resolution mapping of forest carbon stocks in the Colombian Amazon. *Biogeosciences*, *9*, 2683–2696.

Asner, G. P., Hughes, R. F., Varga, T. A., Knapp, D. E., & Kennedy-Bowdoin, T. (2009). Environmental and biotic controls over aboveground biomass throughout a tropical rain forest. *Ecosystems*, *12*, 261–278.

Asner, G. P., Hughes, R. F., Vitousek, P.M., Knapp, D. E., Kennedy-Bowdoin, T., Boardman, J., et al. (2008). Invasive plants transform the three-dimensional structure of rain forests. *Proceedings of the National Academy of Sciences of the United States of America*, *105*, 4519–4523.

Asner, G. P., Kellner, J. R., Kennedy-Bowdoin, T., Knapp, D. E., Anderson, C., & Martin, R. E. (2013). Forest canopy gap distributions in the Southern Peruvian Amazon. *PLoS ONE*, *8*, e60875.

Asner, G. P., Knapp, D. E., Boardman, J., Green, R. O., Kennedy-Bowdoin, T., Eastwood, M., et al. (2012). Carnegie Airborne Observatory-2: Increasing science data dimensionality via high-fidelity multi-sensor fusion. *Remote Sensing of Environment*, *124*, 454–465.

Asner, G. P., Knapp, D. E., Kennedy-Bowdoin, T., Jones, M.O., Martin, R. E., Boardman, J., et al. (2007). Carnegie Airborne Observatory: In-flight fusion of hyperspectral imaging and waveform light detection and ranging (wLiDAR) for three-dimensional studies of ecosystems. *Journal of Applied Remote Sensing*, *1*.

Asner, G. P., & Martin, R. E. (2011). Canopy phylogenetic, chemical and spectral assembly in a lowland Amazonian forest. *New Phytologist*, *189*, 999–1012.

Asner, G. P., Martin, R. E., Knapp, D. E., Tupayachi, R., Anderson, C., Carranza, L., et al. (2011). Spectroscopy of canopy chemicals in humid tropical forests. *Remote Sensing of Environment*, *115*, 3587–3598.

Asner, G. P., Mascaro, J., Muller-Landau, H. C., Vieilledent, G., Vaudry, R., Rasamoelina, M., et al. (2012). A universal airborne LiDAR approach for tropical forest carbon mapping. *Oecologia*, *168*, 1147–1160.

Asner, G. P., Powell, G. V. N., Mascaro, J., Knapp, D. E., Clark, J. K., Jacobson, J., et al. (2010). High-resolution forest carbon stocks and emissions in the Amazon. *Proceedings of the National Academy of Sciences of the United States of America*, *107*, 16738–16742.

Asner, G. P., & Vitousek, P.M. (2005). Remote analysis of biological invasion and biogeochemical change. *Proceedings of the National Academy of Sciences of the United States of America*, *102*, 4383–4386.

Baldeck, C. A., & Asner, G. P. (2013). Estimating vegetation beta diversity from airborne imaging spectroscopy and unsupervised clustering. *Remote Sensing*, *5*, 2057–2071.

Carlson, K. M., Asner, G. P., Hughes, R. F., Ostertag, R., & Martin, R. E. (2007). Hyperspectral remote sensing of canopy biodiversity in Hawaiian lowland rainforests. *Ecosystems*, *10*, 536–549.

Castillo, M., Rivard, B., Sanchez-Azofeifa, A., Calvo-Alvarado, J., & Dubayah, R. (2012). LIDAR remote sensing for secondary tropical dry forest identification. *Remote Sensing of Environment*, *121*, 132–143.

Cho, M.A., Mathieu, R., Asner, G. P., Naidoo, L., van Aardt, J., Ramoelo, A., et al. (2012). Mapping tree species composition in South African savannas using an integrated airborne spectral and LiDAR system. *Remote Sensing of Environment*, *125*, 214–226.

Clark, M. L., Roberts, D. A., & Clark, D. B. (2005). Hyperspectral discrimination of tropical rain forest tree species at leaf to crown scales. *Remote Sensing of Environment*, *96*, 375–398.

Clark, M. L., Roberts, D. A., Ewel, J. J., & Clark, D. B. (2011). Estimation of tropical rain forest aboveground biomass with small-footprint lidar and hyperspectral sensors. *Remote Sensing of Environment*, *115*, 2931–2942.

Colgan, M. S., Baldeck, C. A., Feret, J. B., & Asner, G. P. (2012). Mapping savanna tree species at ecosystem scales using support vector machine classification and BRDF correction on airborne hyperspectral and LiDAR data. *Remote Sensing*, *4*, 3462–3480.

Condit, R., Engelbrecht, B.M. J., Pino, D., Perez, R., & Turner, B.L. (2013). Species distributions in response to individual soil nutrients and seasonal drought across a community of tropical trees. *Proceedings of the National Academy of Sciences of the United States of America*, *110*, 5064–5068.

Drake, J. B., Dubayah, R. O., Knox, R. G., Clark, D. B., & Blair, J. B. (2002). Sensitivity of large-footprint lidar to canopy structure and biomass in a neotropical rainforest. *Remote Sensing of Environment*, *81*, 378–392.

Dubayah, R. O., Sheldon, S. L., Clark, D. B., Hofton, M.A., Blair, J. B., Hurtt, G. C., et al. (2010). Estimation of tropical forest height and biomass dynamics using lidar remote sensing at La Selva, Costa Rica. *Journal of Geophysical Research — Biogeosciences*, *115*.

Feret, J. B., & Asner, G. P. (2012). Semi-supervised methods to identify individual crowns of lowland tropical canopy species using imaging spectroscopy and LiDAR. *Remote Sensing*, *4*, 2457–2476.

Held, A., Ticehurst, C., Lymburner, L., & Williams, N. (2003). High resolution mapping of tropical mangrove ecosystems using hyperspectral and radar remote sensing. *International Journal of Remote Sensing*, *24*, 2739–2759.

Higgins, M.A., Asner, G. P., Perez, E., Elespuru, N., Tuomisto, H., Ruokolainen, K., et al. (2012). Use of landsat and SRTM data to detect broad-scale biodiversity patterns in northwestern Amazonia. *Remote Sensing*, *4*, 2401–2418.

Higgins, M.A., Ruokolainen, K., Tuomisto, H., Llerena, N., Cardenas, G., Phillips, O. L., et al. (2011). Geological control of floristic composition in Amazonian forests. *Journal of Biogeography*, *38*, 2136–2149.

Higgins, M. A., & Ruokolainen, K. (2004). Rapid tropical forest inventory: a comparison of techniques based on inventory data from western Amazonia. *Conservation Biology*, *18*, 799–811.

Ibanez, R., Condit, R., Angehr, G., Aguilar, S., Garcia, T., Martinez, R., et al. (2002). An ecosystem report on the Panama Canal: Monitoring the status of the forest communities and the watershed. *Environmental Monitoring and Assessment*, *80*, 65–95.

John, R., Dalling, J. W., Harms, K. E., Yavitt, J. B., Stallard, R. F., Mirabello, M., et al. (2007). Soil nutrients influence spatial distributions of tropical tree species. *Proceedings of the National Academy of Sciences of the United States of America*, *104*, 864–869.

Jones, M. M., Ferrier, S., Condit, R., Manion, G., Aguilar, S., & Pérez, R. (2013). Strong congruence in tree and fern community turnover in response to soils and climate in central Panama. *Journal of Ecology*, *101*, 506–516.

Kalacska, M., Sanchez-Azofeifa, G. A., Rivard, B., Caelli, T., White, H. P., & Calvo-Alvarado, J. C. (2007). Ecological fingerprinting of ecosystem succession: Estimating secondary tropical dry forest structure and diversity using imaging spectroscopy. *Remote Sensing of Environment*, *108*, 82–96.

Kellner, J. R., Asner, G. P., Vitousek, P.M., Tweiten, M.A., Hotchkiss, S., & Chadwick, O. A. (2011). Dependence of forest structure and dynamics on substrate age and ecosystem development. *Ecosystems*, *14*, 1156–1167.

Kokaly, R. F., Asner, G. P., Ollinger, S. V., Martin, M. E., & Wessman, C. A. (2009). Characterizing canopy biochemistry from imaging spectroscopy and its application to ecosystem studies. *Remote Sensing of Environment*, *113*, S78–S91.

Lefsky, M.A., Cohen, W. B., Parker, G. G., & Harding, D. J. (2002). Lidar remote sensing for ecosystem studies. *Bioscience*, *52*, 19–30.

Legendre, P., & Legendre, L. (1998). *Numerical ecology*.

Leutner, B. F., Reineking, B., Muller, J., Bachmann, M., Beierkuhnlein, C., Dech, S., et al. (2012). Modelling forest alpha-diversity and floristic composition — On the added value of LiDAR plus hyperspectral remote sensing. *Remote Sensing*, *4*, 2818–2845.

Please cite this article as: Higgins, M.A., et al., Linking imaging spectroscopy and LiDAR with floristic composition and forest structure in Panama, *Remote Sensing of Environment* (2014), http://dx.doi.org/10.1016/j.rse.2013.09.032

Lucas, R. M., Lee, A.C., & Bunting, P. J. (2008). Retrieving forest biomass through integration of CASI and LiDAR data. *International Journal of Remote Sensing*, *29*, 1553–1577.

Mascaro, J., Asner, G. P., Muller-Landau, H. C., van Breugel, M., Hall, J., & Dahlin, K. (2011). Controls over aboveground forest carbon density on Barro Colorado Island, Panama. *Biogeosciences*, *8*, 1615–1629.

MICI (1990). *Geología de la República de Panamá*. Dirección General de Recursos Minerales. Ministerio de Comercio e Industrias.

Myneni, R. B., Nemani, R. R., & Running, S. W. (1997). Estimation of global leaf area index and absorbed par using radiative transfer models. *IEEE Transactions on Geoscience and Remote Sensing*, *35*, 1380–1393.

Palmiotto, P. A., Davies, S. J., Vogt, K. A., Ashton, M. S., Vogt, D. J., & Ashton, P.S. (2004). Soil-related habitat specialization in dipterocarp rain forest tree species in Borneo. *Journal of Ecology*, *92*, 609–623.

Ren, D., Leslie, L. M., & Duan, Q. (2012). Landslides caused deforestation. In P. Moutinho (Ed.), *Deforestation around the world*. Shanghai Intech Publishers978-953-51-0417-9.

Salovaara, K. J., Thessler, S., Malik, R. N., & Tuomisto, H. (2005). Classification of Amazonian primary rain forest vegetation using Landsat ETM plus satellite imagery. *Remote Sensing of Environment*, *97*, 39–51.

Sanchez-Azofeifa, G. A., Castro, K., Wright, S. J., Gamon, J., Kalacska, M., Rivard, B., et al. (2009). Differences in leaf traits, leaf internal structure, and spectral reflectance between two communities of lianas and trees: Implications for remote sensing in tropical environments. *Remote Sensing of Environment*, *113*, 2076–2088.

Schmidtlein, S., & Sassin, J. (2004). Mapping of continuous floristic gradients in grasslands using hyperspectral imagery. *Remote Sensing of Environment*, *92*, 126–138.

Schmidtlein, S., Zimmermann, P., Schupferling, R., & Weiss, C. (2007). Mapping the floristic continuum: Ordination space position estimated from imaging spectroscopy. *Journal of Vegetation Science*, *18*, 131–140.

Tuomisto, H., Poulsen, A.D., Ruokolainen, K., Moran, R. C., Quintana, C., Celi, J., et al. (2003). Linking floristic patterns with soil heterogeneity and satellite imagery in Ecuadorian Amazonia. *Ecological Applications*, *13*, 352–371.

Tuomisto, H., Ruokolainen, K., Aguilar, M., & Sarmiento, A. (2003). Floristic patterns along a 43-km long transect in an Amazonian rain forest. *Journal of Ecology*, *91*, 743–756.

Ustin, S. L., Gitelson, A. A., Jacquemoud, S., Schaepman, M., Asner, G. P., Gamon, J. A., et al. (2009). Retrieval of foliar information about plant pigment systems from high resolution spectroscopy. *Remote Sensing of Environment*, *113*, S67–S77.

Wolf, J. A., Fricker, G. A., Meyer, V., Hubbell, S. P., Gillespie, T. W., & Saatchi, S. S. (2012). Plant species richness is associated with canopy height and topography in a neotropical forest. *Remote Sensing*, *4*, 4010–4021.

Please cite this article as: Higgins, M.A., et al., Linking imaging spectroscopy and LiDAR with floristic composition and forest structure in Panama, *Remote Sensing of Environment* (2014), http://dx.doi.org/10.1016/j.rse.2013.09.032